3.1. Introduction

Wear and friction between moving surfaces have to be overcome for the endurance of the machine components. The additives with antifriction and antiwear properties are, therefore, blended with the base lubricant. On account of small size, nano-sized materials are beneficial for quick response at the interface.[1-3] Various types of nanosheets, nanoparticles, and nanocomposites are available in the literature for their tribological properties.[4-7] Among the nanosheets, MoS_2,[8,9] graphene,[10,11,12] and boron nitride[13] have specifically drawn attention owing to the existence of weak Van der Waals forces between the proximal layers, which facilitates shearing under sliding motion.[13,14,15]

Graphene is a two-dimensional hexagonal lattice of sp^2-hybridized carbon atoms. Each carbon atom is bonded to its three neighbors by a sigma bond and one pi bond perpendicular to the plane.[9] Graphene oxide (GO),[11,12] an oxidized form of graphene, consists of oxygen-containing functional groups like epoxide, hydroxy, and carboxylic acid; therefore, it has less sp^2 character/ less graphitic nature[16] or more defects. The load-bearing capacity, wear, and friction-reducing characteristics of graphene oxide /reduced graphene oxide (GO/rGO) are not much commendable. Apart from moderate tribological activity, there are some drawbacks also associated during lubrication like agglomerating and restacking tendencies of the nanosheets, weaker ability for dispersion in the lubricant, and feeble adherence to the interacting surfaces. For improvement of these properties, its functionalization either covalently/non-covalently or both can be performed.[17,18] Several nanocomposites involving non-covalent functionalization by nanoparticles like copper, gold, lanthanum fluoride, zinc oxide, etc. have been narrated for enhanced triboactivity.[19-

[22] The nanocomposite of reduced graphene oxide (rGO) with magnesium-doped zinc oxide nanoparticles,[22] B, N-co-doped rGO with titanium dioxide[23] and amino borate-functionalized rGO further functionalized with copper phthalocyanine nanotubes,[24] have been proclaimed from our laboratory to possess outstanding tribological characteristics. Song and co-workers have reported the tribological behavior of nanocomposite of graphene oxide with MoS_2.[7] Investigations on copper metal matrix composite reinforced by rGO-MoS_2 nanohybrid have shown high activity.[9] Recently, a nanocomposite of rGO, MoS_2, and zirconia/cerium-doped zirconia nanoparticles has been recorded as an excellent friction and wear modifier by us.[25] Since chemical modification of graphene caters manifold advantages, deterrence to agglomeration, and feasibility towards dispersion in various systems[26] along with increased tribological properties[24], it appeared us fascinating to functionalize rGO using nucleophilic substitution reaction. Sulfur compounds, in general, are highly triboactive, methionine was, therefore, intentionally selected for the purpose, forming M-rGO.[16] Methionine is an amino acid; the substitution has occurred at epoxy and carboxylic groups[27] in M-rGO. The graphene oxide is reduced to rGO during the process of functionalization.

Further, MoS_2, a dichalcogenide of tribological importance, consists of the hexagonal plane of molybdenum atoms sandwiched between two hexagonal planes of sulfur atoms in such a way that molybdenum remains covalently bonded to six sulfur atoms (three from each layer) in the trigonal prismatic arrangement.[7,28,29] As discussed above, covalent functionalization of GO may be easily performed due to the presence of functional groups like epoxide, hydroxy, and carboxyl. On the other hand, there are no such functionalities

in MoS_2; therefore, its covalent functionalization is difficult. However, its non-covalent functionalization may be easily brought about by nanoparticles. Chemically capped zinc borate[30] and Fe_3O_4[31] have been used to functionalize MoS_2 to produce nanocomposites showing substantial enhancement in the tribological activity. For preparing the nanocomposite of MoS_2 in the present investigation, yttrium oxide (Y_2O_3) was considered as it is also well known for its tribological activity.[32] Tribological properties of plasma-sprayed Al_2O_3-Y_2O_3 composite coatings and yttria-stabilized zirconia coatings are well documented in the literature.[33,34] Doping of layered yttria by zirconium, lanthanum, and lanthanides, like europium, neodymium is known to enhance the luminescent properties.[35-38] For upgrading the tribological activity of yttria, doping with lanthanum was preferred since doped nanoparticles often show increased tribological activity, for example, calcium, aluminium or yttrium doped zirconia,[39,40] magnesium, copper doped zinc oxide,[41,42] lanthanum doped titania,[43] rhenium doped molybdenum disulfide,[44] titanium doped niobium diselenide.[45] A literature survey[46,47] revealed that doping of lanthanum in yttria was usually between 7 to 10%. In all the cases, the presence of the cubic phase of yttria was confirmed. Samples with 7 and 10% La-doped yttria were therefore prepared. The tribological results were far better for 7%; accordingly, this sample was used further for preparing composites.

Thus, La-Y_2O_3 was used to prepare the nanohybrid with MoS_2. Further, methionine functionalized reduced graphene oxide was appended for the progression of the activity of binary composite (La-Y_2O_3)-MoS_2. Thus, a customized composite of lanthanum-doped yttria NPs with MoS_2 was upgraded with methionine functionalized rGO to attain

excellent tribological performance. Lubricating properties of the as-prepared nano additives, Y_2O_3, La-Y_2O_3, MoS_2, M-rGO, (La-Y_2O_3)-MoS_2 and (La-Y_2O_3)-MoS_2-(M-rGO), were appraised on a four-ball tribo tester following ASTM D4172 and ASTM D5183 standards.

3.2. EXPERIMENTAL SECTION

3.2.1. Materials

The required chemicals of analytical grade were procured for the present investigation.

3.2.2. Syntheses of nano additives

3.2.2.1. Synthesis of yttria and 7% lanthanum-doped yttria nanoparticles

Preparation of yttria and 7% lanthanum-doped yttria nanoparticles was achieved by the auto-combustion method.[48,49] For the preparation of Y_2O_3 NPs, $Y(NO_3)_3.6H_2O$ (3.39g), and citric acid (1.02 g) were dissolved in distilled water (50 mL). The solution was heated at around 230 °C accompanied by uninterrupted stirring till gel was formed. The gel ultimately turned into ash. The calcination of black ash at 600 ^oC in a muffle furnace for 4 h produced Y_2O_3 nanoparticles. Lanthanum-doped (7%) yttria nanoparticles were prepared similarly by using $Y(NO_3)_3.6H_2O$ (3.06g), $La(NO_3)_3.6H_2O$ (0.26g), citric acid (1.0 g) and calcination temperature as 750 ^oC.

3.2.2.2. Synthesis of MoS_2 nanosheets

MoS_2 nanosheets were prepared hydrothermally.[50] A homogeneous solution containing ammonium heptamolybdate, $(NH_4)_6Mo_7O_{24}.4H_2O$ (1.20g) and thiourea $SC(NH_2)_2$ (2.60 g) was prepared in 40 mL of distilled water by ultrasonication for 30 min. The solution was taken in a 200 mL Teflon autoclave, and the temperature was maintained at 180 °C

for 12 h. When the reaction product cooled down to ambient temperature, it was washed with a solvent mixture containing water and ethanol in a 1:1 ratio. Finally, it was dried at 60 °C.

3.2.2.3. Preparation of binary composite, lanthanum-doped Y_2O_3 nanoparticles, and MoS_2 nanosheets

Dispersions of lanthanum-doped Y_2O_3 nanoparticles (0.3g) and MoS_2 nanosheets (0.3g) were prepared separately in 100 mL ethanol by ultrasonication for 2 h at room temperature. The prepared dispersions were mixed under constant stirring. The mixture was sonicated at 70 ^oC and kept for 5 min in the microwave oven at 700 W, which resulted in a black product.[22]

3.2.2.4. Preparation of graphene oxide (GO) and methionine functionalized reduced graphene oxide (M-rGO)

Modified Hummer's method was used to prepare graphene oxide (GO).[26] The GO (0.2g), methionine (0.6g), and equimolar NaOH were taken in distilled water (40 mL) and stirred for 24 h at room temperature. The colloidal dispersion was sonicated for 2 h after the addition of ethanol. It was centrifuged, washed with the ethanol-water mixture, and dried at 60 ^oC.[16]

The formation of M-rGO was confirmed by comparing the Fourier Transform Infrared Spectra of GO and M-rGO, Figure 3.1. The FTIR spectrum of GO exhibits stretching vibrations for the C=O (carboxylic acid), benzenoid C=C, C-OH, C-O-C, and C-O groups at 1715, 1620, 1386, 1220, and 1054 cm^{-1} respectively. A broad peak at 3404 cm^{-1} is attributed to the O-H stretching of absorbed water.[51] Upon functionalization, two new

peaks are observed at 2970 and 2825 cm^{-1}, which are ascribed to the stretching vibrations of the CH_2 group of methionine.[51] The peaks appearing at 1638 and 3164 cm^{-1} are assigned to the C=O and N-H stretching modes of the amide group, respectively.[52] The presence of a peak at 1490 cm^{-1} corresponds to the stretching vibration of amide (-CONH-), demonstrating amide formation during functionalization.[53] The bands at 1723, 1043, and 718 cm^{-1} are accorded with stretching vibrations of C=O(the carboxylic group of methionine), C-N, and C-S, respectively.[16,53,54] Besides, a broad band at 3392 cm^{-1} is also noted due to the O-H and N-H stretching vibrations.[53] Presence of the above bands in the spectrum of M-rGO explicitly, those due to amide, N-H, and C-S groups confirm the covalent functionalization of GO via ring-opening at epoxide group and amide formation at the carboxylic group, leading eventually to the formation of M-rGO.

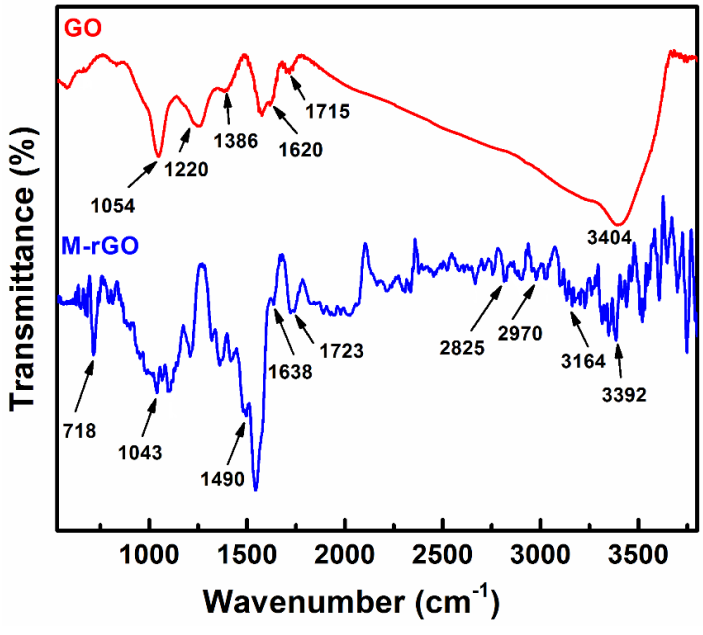

Figure 3.1. FT-IR spectra of the GO and M-rGO

3.2.2.5. Preparation of ternary composite (La-Y_2O_3)-MoS_2-(M-rGO)

The La-Y_2O_3 (0.3g), molybdenum disulfide (0.3g), and M-rGO (0.3g) were dispersed in 100 mL of ethanol via ultrasonication. The resulting prepared dispersion was refluxed at 80 ^oC under vigorous stirring for 24 h. The reaction system was brought down to room temperature, washed with ethanol using centrifugation, and dried.[55] (Scheme 3.1).

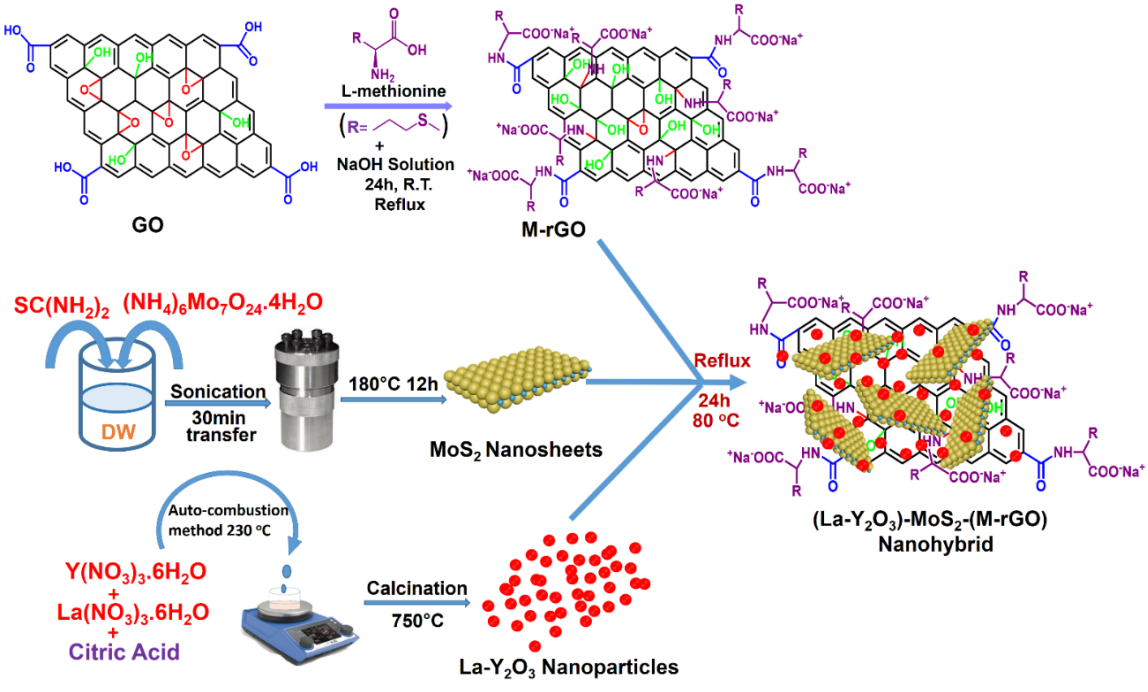

Scheme 3.1: Illustration of synthesis of ternary nanohybrid (La-Y_2O_3)-MoS_2-(M-rGO)

3.2.3. Tribological tests

The test samples were prepared by 1 h sonication of the studied additives, 0.10, 0.15, 0.20, 0.25, 0.30, and 0.35% (w/v) in the base lube paraffin oil (PO). According to the observed data, the optimized concentration could be established as 0.2% w/v for testing of all the additives on a four-ball tester using ASTM-D4172 and ASTM-D5183 standards.

3.3. Results and Discussion

3.3.1. Techniques adopted to characterize the nano additives

For examining the morphological and microstructural characteristics of the nano additives, SEM/HR-SEM images of the additives were recorded. Figure 3.2a-g illustrates HR-SEM images of Y_2O_3 nanoparticles, 7% La-doped Y_2O_3 (La-Y_2O_3) nanoparticles, MoS_2 nanosheets, binary composite (La-Y_2O_3)-MoS_2, methionine functionalized reduced graphene oxide (M-rGO) nanosheets, the ternary nanohybrid, (La-Y_2O_3)-MoS_2-(M-rGO) and EDX spectrum of the ternary nanohybrid respectively. Figures 3.2a and 3.2b exhibit Y_2O_3 and La-Y_2O_3 NPs of almost spherical shape with little agglomeration. In Figure 3.2c, MoS_2 exhibits randomly stacked layered morphology with a flake-like structure. The thickness and size of the nanosheets, indeed affect the lubrication properties. The lesser thickness of the nanosheets assures their better penetration at the rubbing interfaces.[8] The lateral size of nanosheets lies in the range of 150nm to 500nm with a thickness of 10-15nm.

Figure 3.2d depicts MoS_2 nanosheets furbished with La-doped Y_2O_3 NPs. The M-rGO nanosheets can be perceived in Figure 3.2e. The M-rGO comprises thin, smooth, and folded nanosheets with lateral size ranging from 500nm to 6µm and thickness between 13-17nm. Figure 3.2f presents the distinct appearance of La-Y_2O_3 NPs on both types of nanosheets, MoS_2 and M-rGO. The EDX spectrum of (La-Y_2O_3)-MoS_2 exhibits clear signals for yttrium, lanthanum, molybdenum, oxygen, and sulfur. The presence of these elements furnishes evidence in favor of the formation of the binary composite. The corresponding spectrum is shown in Figure 3.3. The EDX spectrum of the ternary

nanocomposite is displayed in Figure 3.2g. The appearance of distinct peaks for the elements carbon and nitrogen besides yttrium, lanthanum, molybdenum, oxygen, and sulfur substantiate the existence of (La-Y_2O_3)-MoS_2-(M-rGO).

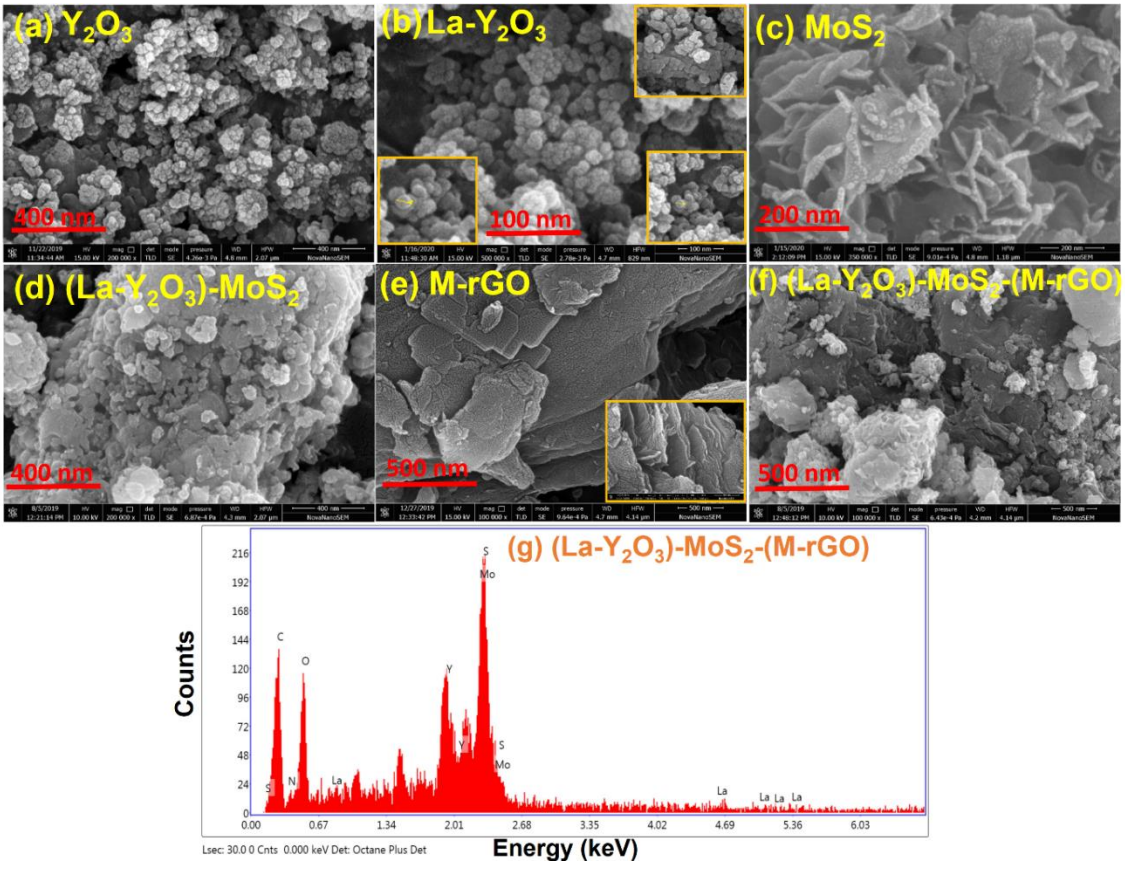

Figure 3.2. HR-SEM images of (a) Y_2O_3, (b) La-Y_2O_3, (c) MoS_2, (d) (La-Y_2O_3)-MoS_2 (e) M-rGO, (f) (La-Y_2O_3)-MoS_2-(M-rGO), and (g) EDX spectrum of (La-Y_2O_3)-MoS_2-(M-rGO)

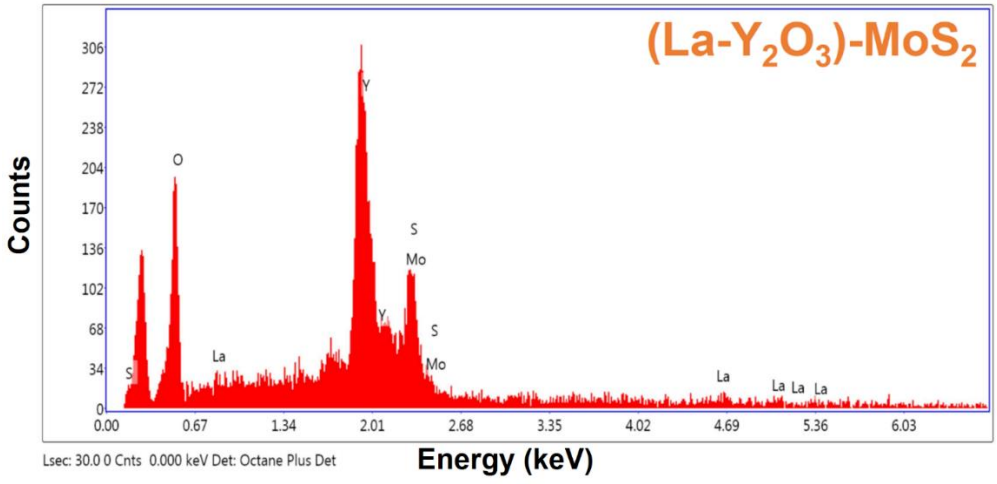

Figure 3.3. EDX spectrum of (La-Y_2O_3)-MoS_2

The TEM/HR-TEM images of the nanomaterials have also been documented for a better comprehension of their morphology and put together in Figure 3.4a-f. The TEM images of Y_2O_3 and La- Y_2O_3 NPs are displayed in Figure 3.4a and b, respectively. Doping has resulted in size reduction as well.[41] The TEM and HR-TEM images of MoS_2 nanosheets are shown in Figure 3.4c and c_1, respectively. The distance between two adjacent layers of MoS_2 (002plane) is calculated to be 0.626 nm.[8,56] The crystalline nature of MoS_2 is apparent from its SAED pattern. It is a noteworthy feature of HR-TEM of M-rGO, Figure 3.4d_1 that the interlayer distance of the (002) plane has increased to 0.337nm from rGO (0.334nm) after functionalization.[22] The increase in interlayer distance is indicative of increased sp^3 character due to functionalization. The TEM and HR-TEM images of the ternary nanocomposite (La-doped Y_2O_3)-MoS_2-(M-rGO) shown in Figure 3.4f and f_1 divulge the co-existence of isolated MoS_2 and M-rGO nanosheets together with La-Y_2O_3 NPs adorned over them. The lattice fringes of La-Y_2O_3, corresponding to the (222) plane are observed as 0.31nm.[57] The increased interlayer distance of M-rGO (0.370 nm) and

MoS_2 (0.637 nm)[9] in the ternary nanohybrid is a prominent feature of the HR-TEM image of the ternary nanohybrid.

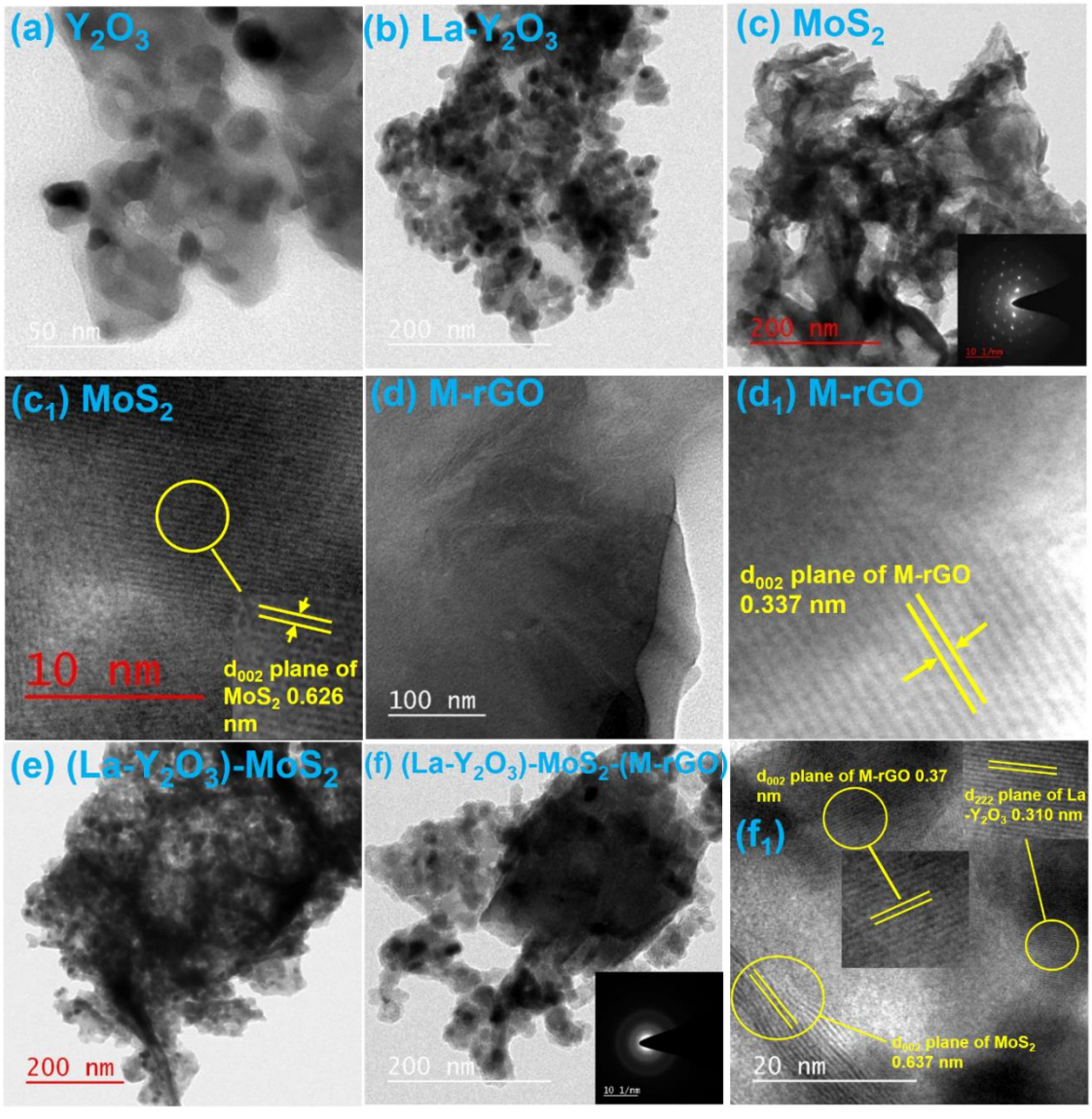

Figure 3.4. TEM images of (a) Y_2O_3, (b) La-Y_2O_3, (c) MoS_2, (d) M-rGO, (e) (La-Y_2O_3)-MoS_2, (f) (La-Y_2O_3)-MoS_2-(M-rGO) and HR-TEM images of (c_1) MoS_2, (d_1) M-rGO, and (f_1) (La-Y_2O_3)-MoS_2-(M-rGO)

The NPs, indeed, helped in segregating the layers and averted their orderly heaping. The nanosheets and NPs have reciprocated each other in impeding agglomeration. Thus, it may be inferred that the nanoparticles act as spacers[25,31,58] between M-rGO and MoS_2 layers and alleviate their restacking.[20,25,31,58] Figure 3.5a reveals the particle size histogram for Y_2O_3 and La-Y_2O_3 nanoparticles obtained from TEM studies. Accordingly, the average size of NPs may be considered as 19 and 14 nm, respectively.

The X-ray diffraction (XRD) patterns of the additives MoS_2, M-rGO, Y_2O_3, La-Y_2O_3, (La-Y_2O_3)-MoS_2 and (La-Y_2O_3)-MoS_2-(M-rGO) are presented in Figure 3.5b. The peak characteristic for the (001) plane of GO at 11° diffraction angle is conspicuously absent in the XRD pattern of M-rGO.[7,59] The absence of the peak in M-rGO, as well as binary and ternary nanohybrids, straightway corresponds to the formation of reduced graphene oxide. A broad peak observed at 24.5° corresponding to the (002) plane of rGO is also identified in the diffraction patterns of M-rGO and the nanohybrids.[59] The diffraction peaks of Y_2O_3 could be indexed for the cubic phase according to JCPDS file no. 083-0927.[48] The intense peaks at 29.2°, 33.7°, and 48.4° correspond to (222), (400), and (440) planes, respectively.[48] The cubic phase extends to exist in the diffraction pattern of La-Y_2O_3 as no new peak is observed for lanthanum.[36,38] The existence of the cubic phase demonstrates that lanthanum is doped in yttria. The same cubic phase is carried over in binary and ternary nanohybrids. The crystallite size by the Debye Scherer equation was found to be 21 nm for Y_2O_3 and 13 nm for La- Y_2O_3.

Based on JCPDS no. 37-1492 and 77-1716, the hexagonal structure of MoS_2 could be identified. The diffraction peaks at 14.3°, 33.6°, 39.4°, and 59.4° accorded with (002),

(100), (103), and (110) planes, respectively.[8,31] The 2-dimensional layered structure was assured because of the sharp and robust peak for the (002) plane.[8] The interlayer spacing of the (002) plane was found to be 0.626 nm, which is following the TEM results.[8,56] The hexagonal phase structure of MoS_2 is maintained in the binary as well as ternary nanohybrids. However, there is a noticeable reduction in the intensity of the peak due to the (002) plane successively in binary and ternary nanohybrids. There is a significant enhancement in the interlayer distance of (002) plane in binary and ternary composites to 0.637 nm,[9,58] which is symptomatic of the interaction of the constituents of the binary/ternary nanohybrids with each other. The presence of sharp, polycrystalline rings along with strong diffraction spots in the selected area diffraction pattern (SEAD) of the ternary nanohybrids is indicative of high crystallinity.

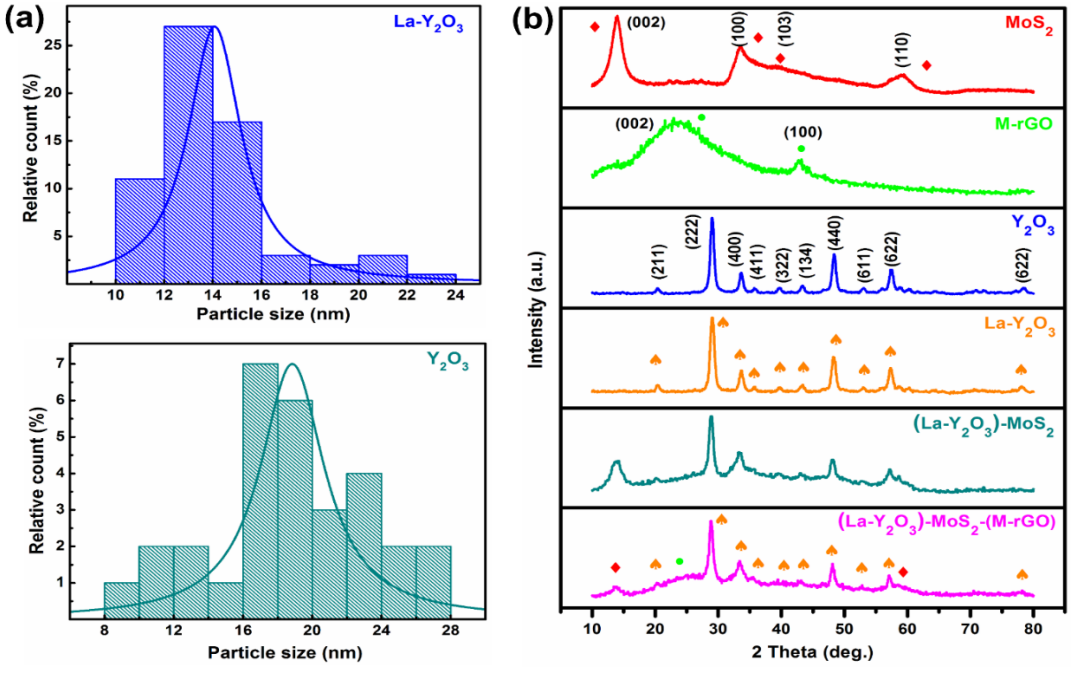

Figure 3.5. (a) The particle size histogram for Y_2O_3 and La-Y_2O_3 nanoparticles obtained from TEM studies, (b) XRD patterns of as-prepared nano additive

Raman spectra of M-rGO, MoS_2, and (La-Y_2O_3)-MoS_2-(M-rGO) were recorded using 633 nm of laser excitations. The corresponding spectra are displayed in Figure 3.6. In the case of the Raman spectrum of La-Y_2O_3 nanoparticles, Figure 3.6a, several peaks are observable. A peak of high scattering intensity represents the Fg mode at 376 $cm^{-1,}$ and few minor peaks at 330.5, 429.3, 464.1, 532, 560.1, and 596.6 cm^{-1}.[60] Most of the peaks of La-Y_2O_3 with reduced intensity could be marked in the spectrum of the ternary composite, Figure 3.6c.

In the Raman spectrum of MoS_2, Figure 3.6b, two bands of high intensity are identified at 378.7 and 405.3 cm^{-1} corresponding to E^1_{2g} and A_{1g} modes, respectively.[8] The former mode conforms to the displacement of molybdenum and sulfur atoms in the layer itself, whereas the latter one signifies their out of layer displacements. The two modes were found to be separated by 27.6 cm^{-1} suggesting a multi-layered structure. The magnitude of separation is associated with a number of layers; the lesser the separation, a number of layers is also lesser.[8] The spectrum of the ternary nanohybrid exhibits these modes with reduced intensity, Figure 3.6c. The spectrum of M-rGO, as an inset in Figure 3.6c, exhibits intense peaks at 1347.5 and 1573.4 cm^{-1} ascribed to D and G bands, respectively.[26,27] The D band is a breathing mode of A_{1g} symmetry and correlates with the magnitude of defects in terms of sp^3/sp^2 hybridization. The G band appears as a consequence of phonon mode of E_{2g} symmetry and comprehends an ordered arrangement of sp^2-hybridized carbon atoms. Besides the position of these bands, the proportion of their intensity I_D/I_G is of paramount significance. The values of I_D/I_G being 0.92 for rGO,[22] 0.97 for M-rGO, and 1.25 in ternary nanocomposite are conclusive of an increase in sp^3

character after functionalization with methionine and formation of ternary nanohybrid, Figure 3.6c.

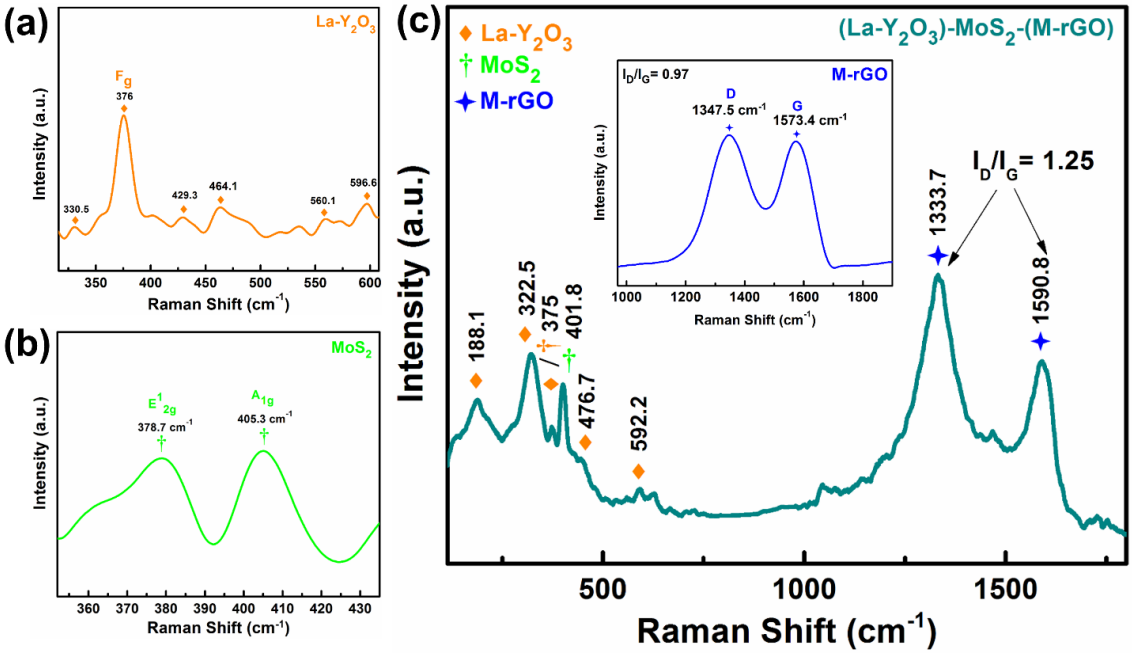

Figure 3.6. Raman spectra of (a) La-Y_2O_3, (b) MoS_2, (c) ternary composite (La-Y_2O_3)-MoS_2-(M-rGO) (inset showing spectra of M-rGO)

The ternary composite (La-Y_2O_3)-MoS_2-(M-rGO) has been characterized by XPS studies to establish the chemical forms of the constituent elements. The survey spectrum, Figure 3.7a, establishes the presence of constituent elements as carbon, oxygen, nitrogen, sulfur, yttrium, molybdenum, and lanthanum. For the deconvolution of the core level spectra, XPS peak fit software has been applied. The deconvoluted core level spectra of C1s, O1s, N1s, S2p, Mo ($3d_{5/2}$ and $3d_{3/2}$), Y($3d_{5/2,}$ and $3d_{3/2}$), and La are depicted in Figure 3.7b-h, respectively. Several peaks are observed in the C1s spectrum, Figure 3.7b at binding energy 284.7, 285.3, 285.9, 286.8, 287.8, and 289.5eV, which could be attributed to C=C,

C-O, C-N, C-S, C=O and –NH-C=O bonds of M-rGO.[19,22,61,62] The spectrum of O 1s, Figure 3.7c exhibits three peaks for M-O bonds of metal oxides [Y-O and La-O], C=O, and C-O at 529.7, 530.8 and 531.8 eV, respectively.[43,57,63]

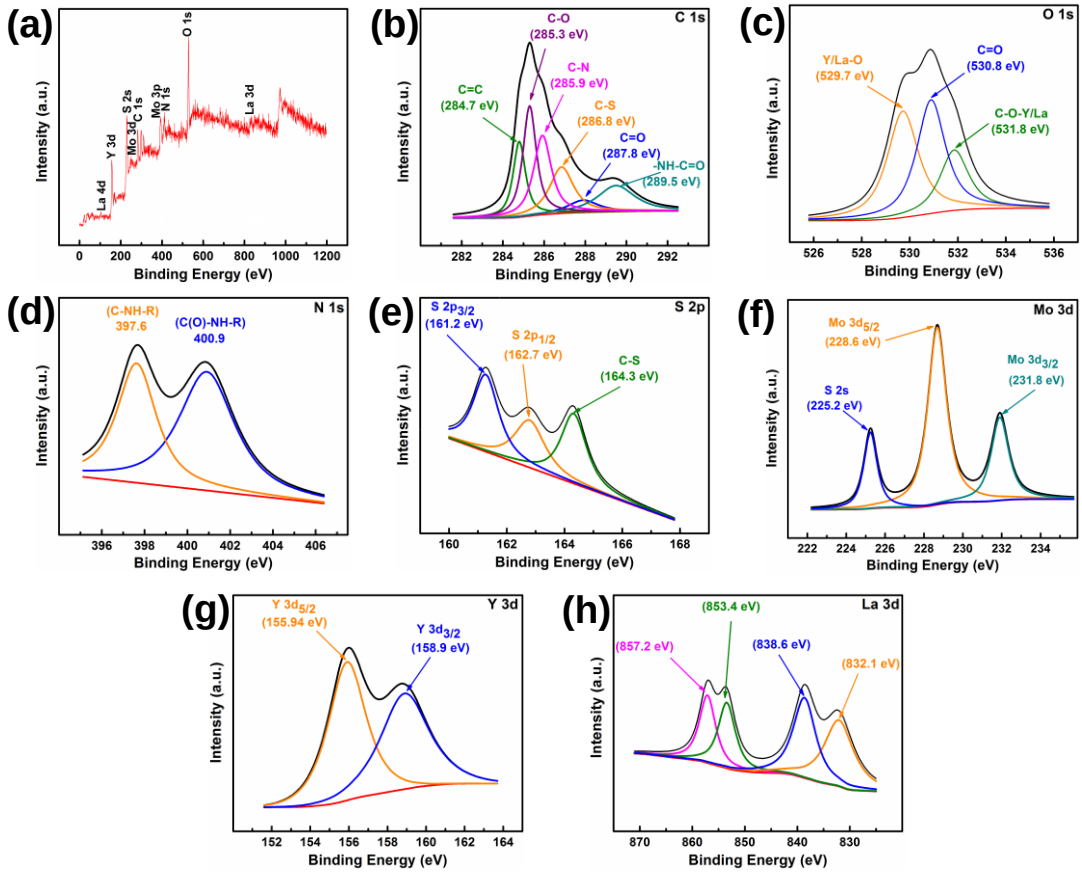

Figure 3.7. Survey spectrum (a) and deconvoluted XPS images of (La-Y_2O_3)-MoS_2-(M-rGO) nanocomposite: (b) C 1s, (c) O 1s, (d) N 1s, (e) S 2p, (f) Mo 3d, (g) Y 3d and (h) La 3d spectra

In the N 1s spectrum, Figure 3.7d, two peaks are observable at binding energy 397.6 and 400.9 eV corresponding to C-NHR and C(O)-NH-R respectively confirming the reaction of -NH_2 group of methionine with epoxide ring and carboxylic group of GO.[19] The S 2p spectrum, Figure 3.7e displays peaks at 161.2 and 162.7, and 164.3 eV according to S

$2p_{3/2}$ and S $2p_{1/2}$ and C-S respectively.[8,62] In the spectrum of molybdenum, Figure 3.7f, Mo $3d_{5/2,}$ and Mo $3d_{3/2}$ could be allocated at 228.6 and 231.8 eV, respectively. The oxidation state (IV) for Mo is identified from the Mo 3d spectrum while S^{2-} is confirmed from the S 2p spectrum. Both together match with the MoS_2 nanosheet. Besides this, an additional peak appearing at 225.2 eV has been indexed for S 2s.[8] The intense peaks corresponding to Y $3d_{5/2}$ and $3d_{3/2}$ are visible in the core level spectrum of yttrium, Figure 3.7g at 155.94 and 158.9 eV, respectively.[37,57] The peaks apparent in the La 3d spectrum, Figure 3.7h at binding energy 832.1, 838.6, 853.4, and 857.2 eV confirm lanthanum as La_2O_3.[21,43,64,65] The presence of characteristic peaks for all individuals signifies the formation of the ternary composite.

3.3.2. Assessment of tribological behavior of nano additives in paraffin oil

3.3.2.1. Dispersion stability

Apart from tribological activity, the stability of dispersions of nano additives is necessarily desired. The determination of dispersion stability can be accomplished by recording the absorbance of the blends (UV/visible spectroscopy) in the range of 200-800 nm every 12 h within 48 h. The blends of the optimized concentration of the additives (0.2% w/v) in PO were 10 times diluted, and their initial absorbance values were noted. After every 12 h, the absorbance data were collected until 48 h. Figure 3.8a delineates the change of relative absorbance against settling time for all the synthesized additives. In general, the relative absorbance goes down with time, but the amount of reduction is quite small. The ternary nanohybrid (La-Y_2O_3)-MoS_2-(M-rGO) shows minimum reduction and maximum stability. However, other additives possess sufficient stability

too, as the relative absorbance, in general, goes up to 0.7, which is not that low.

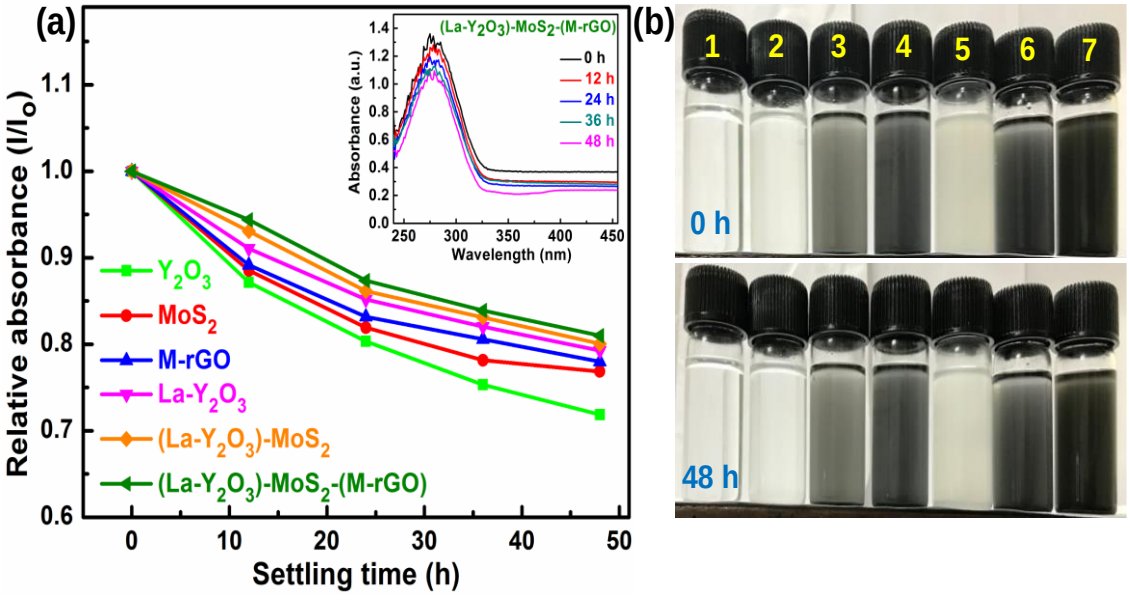

Figure 3.8. (a) Dispersion stabilities of base oil containing Y_2O_3, MoS_2, M-rGO, La-Y_2O_3, (La-Y_2O_3)-MoS_2 and (La-Y_2O_3)-MoS_2-(M-rGO) studied by UV-vis spectrophotometry (inset showing the decrease in absorbance of 278 nm band against time) and (b) Optical photographs of (1) plain PO, and PO with dispersed nano additives (2) Y_2O_3, (3) MoS_2, (4) M-rGO, (5) La-Y_2O_3, (6) (La-Y_2O_3)-MoS_2, and (7) (La-Y_2O_3)-MoS_2-(M-rGO) at zero time and after 48 hours

There are several examples in the literature[66,67] in which NP grafted on graphene nanosheets have been used to increase the dispersibility of graphene. These NPs act as spacers and hinder the stacking of graphene. The composite of rGO/MoS_2 has also been reported to have higher dispersibility than rGO or MoS_2 alone. The whole phenomenon can be explained by steric stabilization[68], according to which the repulsive force is generated by the grafted particle against the van der Waals forces of attraction towards

the approaching particle. Thus, a balanced state is reached, and the agglomeration of the particles is prevented, resulting in enhancing the dispersibility.

The absorbance pattern of a typical additive, the ternary one, has been shown in the inset of Figure 3.8a. It is evident that the additive absorbs at 278 nm and absorbance declines to around 0.7 amidst 48h. Photographs of dispersions in the beginning and after 48h are displayed in Figure 3.8b.

3.3.2.2. Evaluation of Optimized concentration of the additives

The concentration is an important parameter that affects the tribological properties. The blends of the additives with concentrations as 0.00, 0.10, 0.15, 0.20, 0.25, 0.30, and 0.35% w/v in PO were tested at 392 N applied load for 60 min, and the obtained mean wear scar diameters (MWD) are depicted in Figure 3.9a. As compared to plain oil, MWD drops fairly in the presence of blends of additives for each concentration. The drop in MWD increases throughout from blank oil, 0.10, 0.15 to 0.20% w/v in every case. Beyond this concentration, it increases considerably for all the additives. Thus, 0.20% w/v is treated as the optimized concentration for tribological testing of all the additives. Among the additives, MWD is obtained in decreasing order from Y_2O_3, MoS_2, M-rGO, La-Y_2O_3, (La-Y_2O_3)-MoS_2, and finally to (La-Y_2O_3)-MoS_2-(M-rGO). Since the reduction in MWD is directly correlated with enhanced tribological performance, ternary nanohybrid appears to be the best performer.

3.3.2.3. Friction and wear modifying the behavior of the additives

The antiwear tests of base oil and its blends with the synthesized additives at the optimized concentration of 0.20% w/v were performed according to ASTM D4172

standards; 1200 rpm, 392 N load, and 60 min duration. Figure 3.9b portrays a bar diagram for two primarily significant tribological parameters simultaneously, MWD and the average coefficient of friction (COF). The MWD declines continuously from plain oil (0.735mm) in the presence of various additives, Y_2O_3 (15.96%), MoS_2 (19.50%), M-rGO (23.60%), La-Y_2O_3 (29.33%). The reduction enlarges further for binary composite (La-Y_2O_3)-MoS_2 (36.15%) and finally for (La-Y_2O_3)-MoS_2-(M-rGO) (44.70%).

For the average life span of machine components, the COF between the adjacent surfaces in motion has to be minimized. The alteration of COF as a function of time for base oil with or without additives under ASTM D4172 conditions is illustrated in Figure 3.9c. An overview of the Figure demonstrates that the COF is high in the beginning in every case since there is no tribofilm. As the formation of tribofilm initiates, the COF lowers down. After the formation of tribofilm, it becomes stabilized. However, in the case of PO and yttria, a large unstable amplitude of COF can be seen in Figure 3.9c. Indeed, poor adsorption of oil or oil blended with yttria on the ball surface might have resulted in giving such behavior. Moreover, in the case of (La-Y_2O_3)-MoS_2-(M-rGO), it is almost approaching to be stabilized after 1 h. Regarding the relative ordering of different additives, average COF has behaved analogously to MWD. Thus, the COF of paraffin oil without additives (0.0756) has undergone huge depletion when its admixtures with additives are used; Y_2O_3 (12.43%), MoS_2 (31.58%), M-rGO (37.48%), La-Y_2O_3 (40.74%), (La-Y_2O_3)-MoS_2 (51.32%) and (La-Y_2O_3)-MoS_2-(M-rGO) (64.69%). Certainly, the high-level performance of the ternary nanohybrid as a wear and friction modifier cannot be denied. The individuals La-Y_2O_3 (NPs) and MoS_2, M-rGO nanosheets

have interacted significantly to produce efficient tribofilm, which has successfully separated the mating surfaces giving fruitful results for MWD and COF.

For evaluation of wear rate, the MWD values were listed after every 15 min up to 1.5h under 392 N load. The parameter, mean wear volume (MWV), was calculated from the MWD values, and a graph was plotted between MWV and time, Figure 3.9d. The wear rate was obtained using a linear regression model.[22] The wear rates in the range of 0-0.75 h were treated as running-in period and the rest as steady-state period.[22,23,69] Figures 3.10 and 3.11 reveal the associated plots for wear rates.

Like MWD and average COF values here also running-in and steady-state wear rates are very large for base lube alone. Its admixtures with additives bring about adequate reduction to these values. The extent of reduction in wear rates for the tested additives verifies the trend obtained from MWD and COF.

The respective values of running-in and steady-state wear rates ($10^{-4}\times mm^3/h$) for PO and its blends are; PO (84,53), Y_2O_3 (36,15), MoS_2 (31,8), M-rGO (22,7), La-Y_2O_3 (16,5), (La-Y_2O_3)-MoS_2 (13,3), (La-Y_2O_3)-MoS_2-(M-rGO) (9,1).

As per supposition, the ternary nanohybrid shows the lowest value for running-in and steady-state wear rates, proving to be the potential wear and friction modifier.

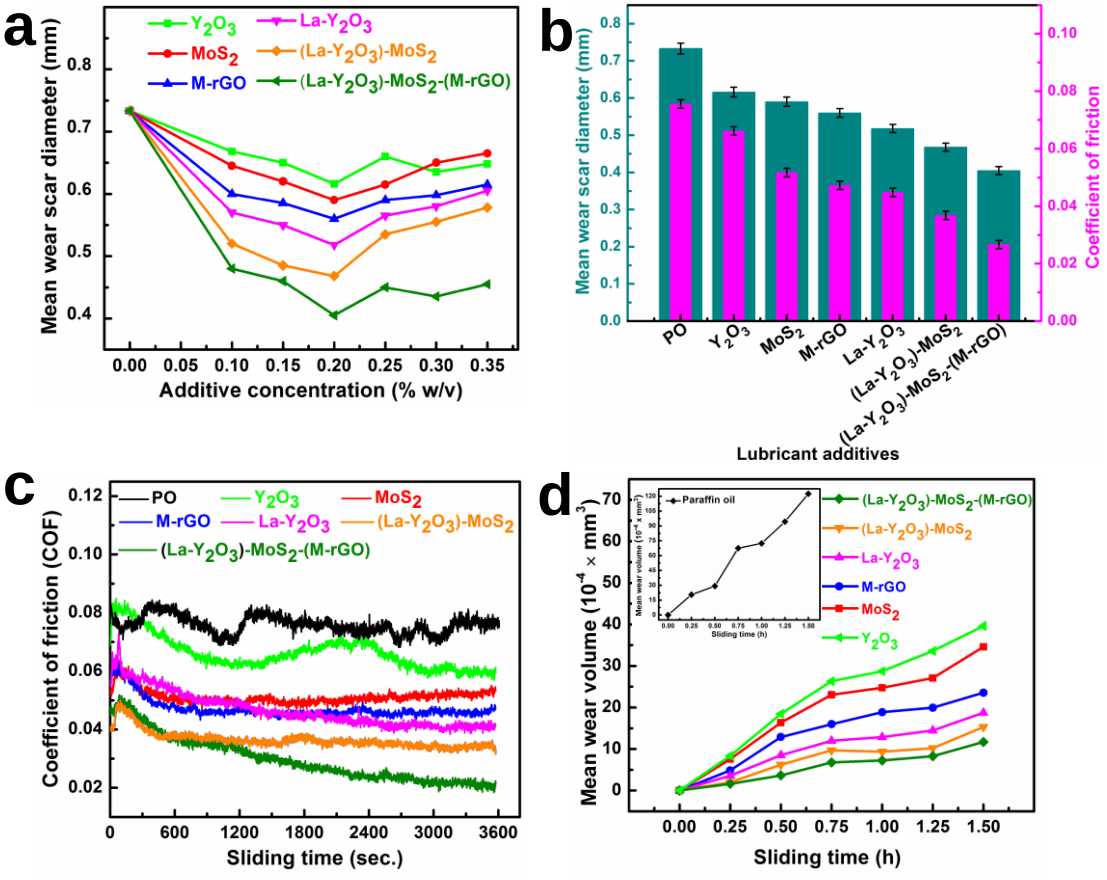

Figure 3.9. (a)Variation of mean wear scar diameter for the paraffin oil as a function of additive concentration at 392 N applied load for 60 min duration (b) mean wear scar diameter and the average coefficient of friction (c) coefficient of friction as a function of sliding time (d) variation of mean wear volume with sliding time for paraffin oil without (given in inset) and with 0.2% w/v of different nano additives for 1.5 h test duration

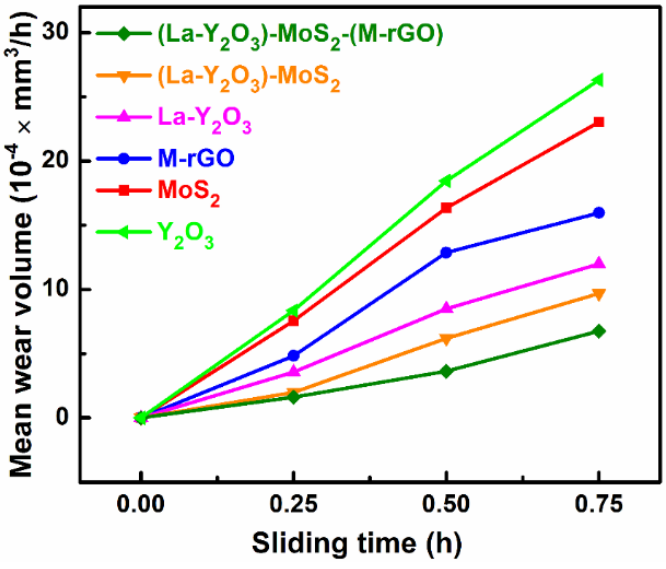

Figure 3.10. Determination of running-in wear rate by varying mean wear volume with time (h) for paraffin oil containing (0.2% w/v) nano additives at 392 N applied load

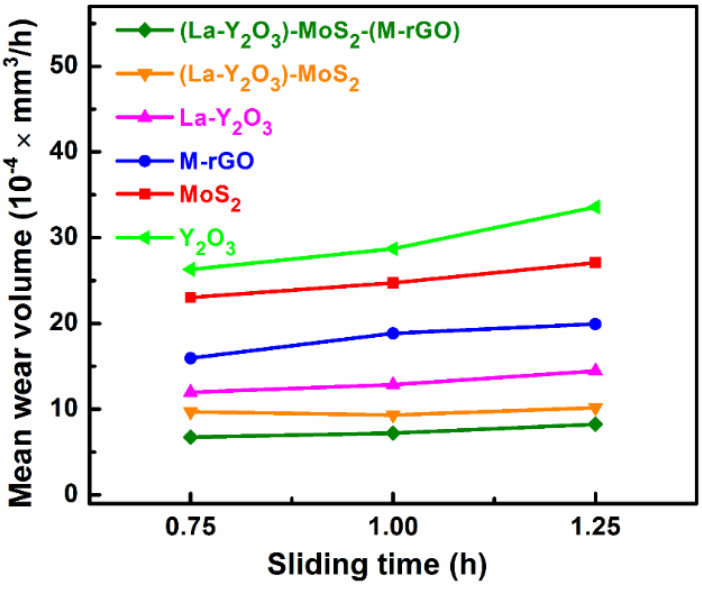

Figure 3.11. Determination of steady-state wear rate by varying mean wear volume with time (h) for paraffin oil containing (0.2% w/v) nano additives at 392 N applied load

3.3.2.4. Load bearing capacity

The load-bearing capacity of the plain oil and the blends was evaluated by load ramp test according to ASTM D-5183 test norms. At first, the test was conducted under the conditions, 392 N load, 600 rpm, 75 ^{o}C temperature, and 60 min duration, assuming that the running-in period is over. It was further continued with successive addition of 98 N load after 10 min gap till the seizure load is reached. Figure 3.12 denotes the plots of frictional torque against time and load together for base lube alone and with additives.

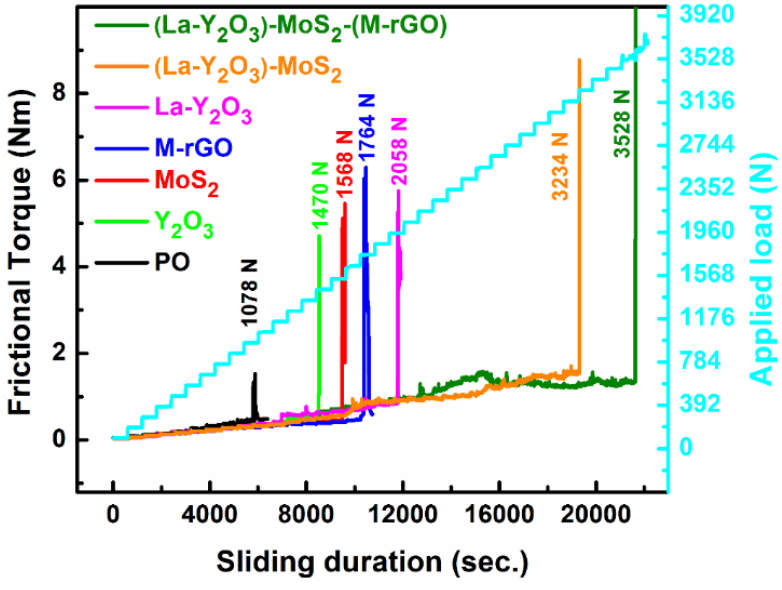

Figure 3.12. Variation of frictional torque as a function of stepwise loading and time for PO in absence and presence of different nano additives: sliding speed, 600 rpm; temperature, 75 ^{o}C; concentration of additives, 0.2% w/v

As apparent from the Figure, the seizure of the mating surfaces is noted at 1078 N, which means the tribofilm is not strong enough to bear the load. However, when additives are appended, tribofilm fails at comparatively much higher loads; Y_2O_3 (1470 N), MoS_2

(1568 N), M-rGO (1764 N), La-Y_2O_3 (2058 N), (La-Y_2O_3)-MoS_2 (3234 N) and (La-Y_2O_3)-MoS_2-(M-rGO) (3528 N). It seems unusual that the load-bearing capacity of rGO has adequately increased from 980 N to 1764 N in M-rGO. [22] The adherence of M-rGO has considerably enhanced from plain rGO. Thus, M-rGO has contributed positively towards the load-bearing capacity of the ternary composite (La-Y_2O_3)-MoS_2-(M-rGO).

3.3.2.5. Worn surface morphological studies

Morphology of the wear path for the only base lube or with the additives has been examined after ASTM D4172 test by surface techniques, SEM and AFM. The obtained SEM images are illustrated in Figure 3.13a. When only plain oil is used, the surface seems to be highly grooved. Conversely, evenness of the surface is improved on the addition of additives. The surface improvement is genuinely in the order of tribo characteristics of the studied blends. The inset of the Figure includes MWD for plain oil and oil-containing additives. The diminution in MWD is conspicuous; plain oil (0.735mm), Y_2O_3 (0.616mm), MoS_2 (0.590mm), M-rGO (0.560mm), La-Y_2O_3 (0.518mm), (La-Y_2O_3)-MoS_2 (0.468mm) and (La-Y_2O_3)-MoS_2-(M-rGO) (0.405mm). The attrition in MWD is concordant with the amelioration of the surfaces.

Elemental composition of the wear scar surface in the presence of the ternary nanocomposite (La-Y_2O_3)-MoS_2-(M-rGO) has been acquired by EDX analysis and revealed in Figure 3.13b. The existence of all the constituent elements, C, O, N, S, Y, La, and Mo, validates their active participation in tribofilm formation to give excellent tribological properties.

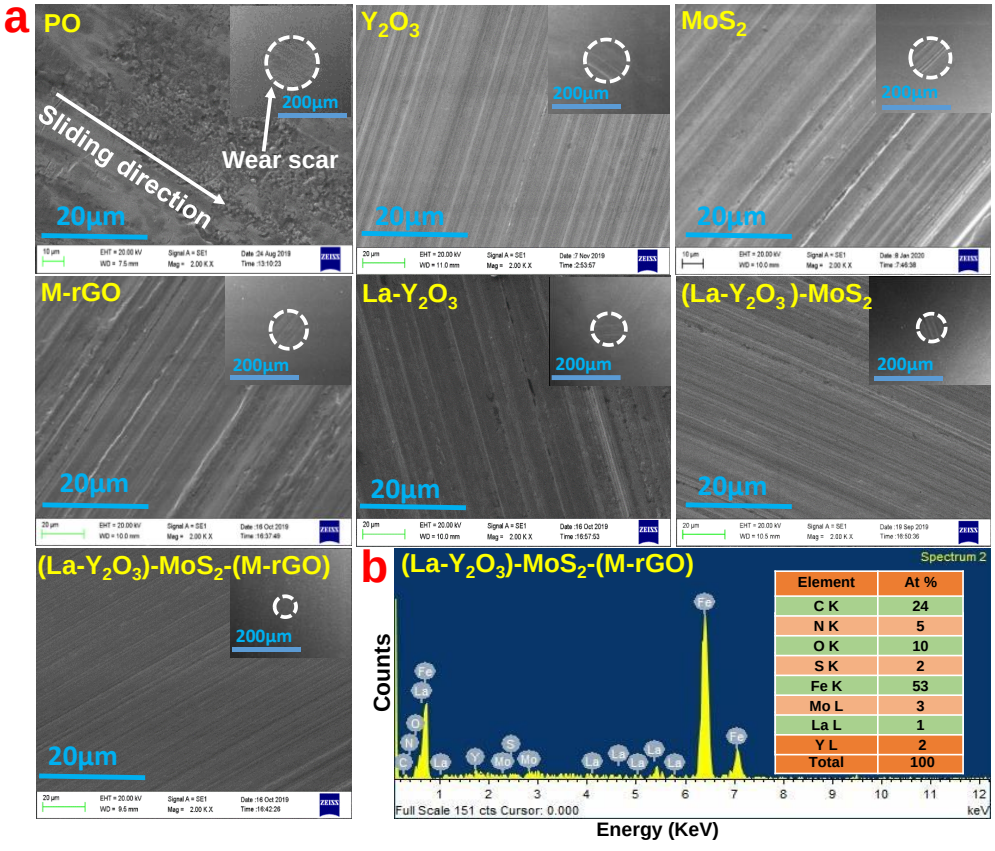

Figure 3.13. (a) SEM micrographs (inset: full view of wear scar at 100X, wear scar surface at 2.00 KX magnification) of the worn steel surface lubricated with paraffin oil with and without different nano additives (0.2% w/v) for 60 min test duration at 392 N applied load (b) EDX spectra of worn surface lubricated with PO blended with 0.2% w/v (La-Y_2O_3)-MoS_2-(M-rGO) nanohybrid at 392 N applied load

The surface of the wear scar has been investigated by AFM studies as well. Figure 3.14 describes *2D* and *3D* images of the worn surfaces along with roughness data in the form of Rq and Sq. The Rq and Sq values for the oil alone (Rq 919 nm, Sq 626 nm) experience massive degradation when mixed with various nano additives; Y_2O_3 (Rq 419 nm, Sq 298 nm), MoS_2 (Rq 275 nm, Sq 247 nm), M-rGO (Rq 189 nm, Sq 213 nm), La-Y_2O_3 (Rq 170

nm, Sq 216 nm), (La-Y_2O_3)-MoS_2 (Rq 97 nm, Sq 164 nm) and (La-Y_2O_3)-MoS_2-(M-rGO) (Rq 30 nm, Sq 65 nm). Thus, the roughness data obtained from AFM studies also endorse the tribological data. Besides this, the other roughness parameters like Sa, Sq, Sy, Sp, Sv, Sm, Ra, Rq, Ry, Rp, Rv, and Rm also corroborated the tribological results. These data are summarized in Table 3.1.

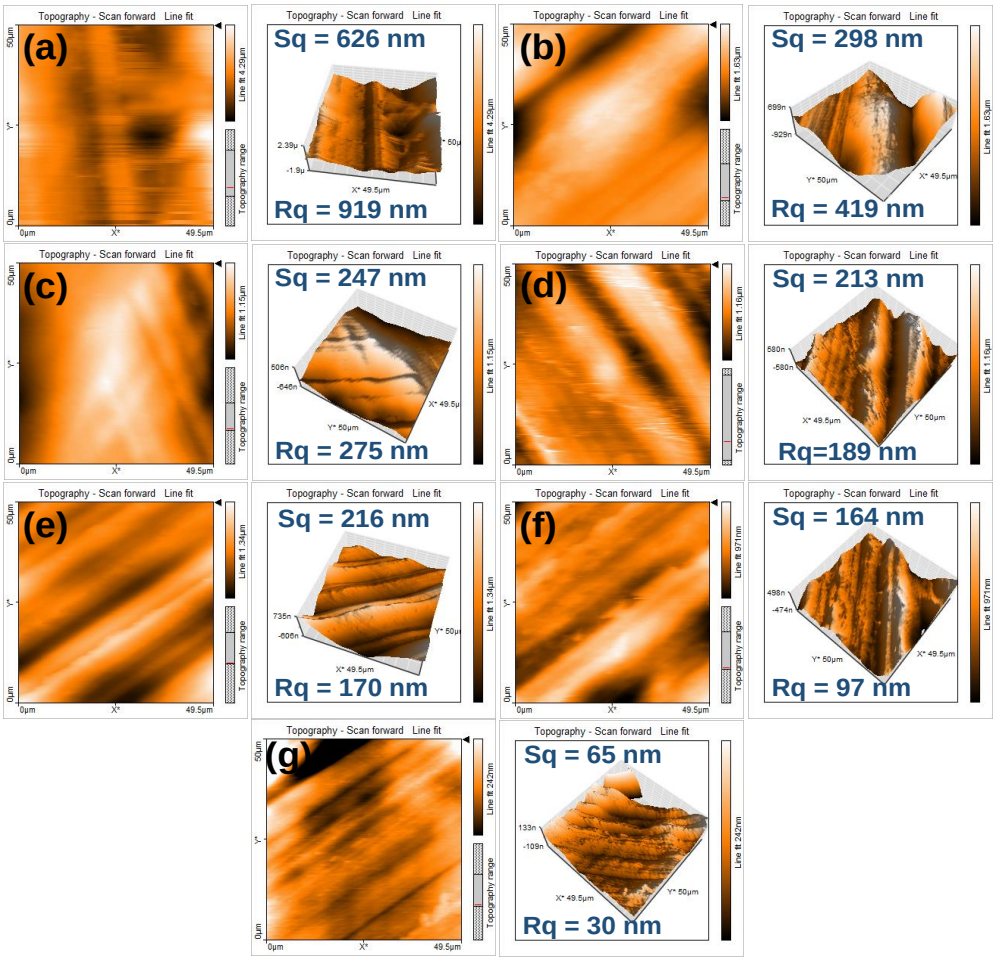

Figure 3.14. *2D* and *3D* AFM images of the worn steel surface lubricated with blank paraffin oil (PO) and blends of PO with 0.2% w/v nano additives at 392 N applied load: (a) paraffin oil, (b) Y_2O_3, (c) MoS_2, (d) M-rGO, (e) La-Y_2O_3, (f) (La-Y_2O_3)-MoS_2, and (g) (La- Y_2O_3)-MoS_2-(M-rGO)

Table 3.1. Surface roughness parameters obtained from the digital processing software of AFM (Nanosurf-basic Scan-2) for different additives after the antiwear test

Surface roughness parameter	Sq (nm)	Rq (nm)	Sa (nm)	Ra (nm)	Sy (nm)	Ry (nm)	Sp (nm)	Rp (nm)	Sv (nm)	Rv (nm)	Sm (pm)	Rm (pm)
PO	626	919	488	771	4363	3255	2611	2060	-1752	-1195	129	-129
Y_2O_3	298	419	231	369	1642	1469	709	550	-932	-919	83	-327
MoS_2	247	275	212	232	1136	1047	514	460	-622	-586	95	-254
M-rGO	213	189	173	146	1418	785	864	292	-553	-392	117	-201
La-Y_2O_3	216	170	171	142	1274	617	730	269	-544	-348	147	-109
(La-Y_2O_3)-MoS_2	164	97	127	82	961	404	466	232	-495	-172	126	-109
(La-Y_2O_3)-MoS_2-(M-rGO)	65	30	43	24	739	115	402	55	-337	-60	116	-108

(Where, S = Areal roughness, and R = Linear roughness parameters).

Sq = root mean square height, Rq = root mean square line

Sa = Arithmetical mean height, Ra = Arithmetic mean line

Sy = Maximum height of the surface, Ry = Maximum height of the profile

Sp = Maximum peak height, Rp = Maximum profile peak height

Sv = Maximum valley depth, Rv = Maximum profile valley depth

Sm = Mean width area, Rm = Mean width line

3.3.2.6. Characterization of the tribochemical film

The worn surface lubricated with ternary composite (La-Y_2O_3)-MoS_2-(M-rGO) has been characterized by XPS studies to detect the chemical state of the underlying elements. For the deconvolution of the core level spectra, XPS peak fit software has been applied. The

deconvoluted core level spectra of C1s, O1s, N1s, S 2p, Mo ($3d_{5/2}$ and $3d_{3/2}$), and Y ($3d_{5/2}$ and $3d_{3/2}$), La and Fe are portrayed in Figure 3.15a-h, respectively.

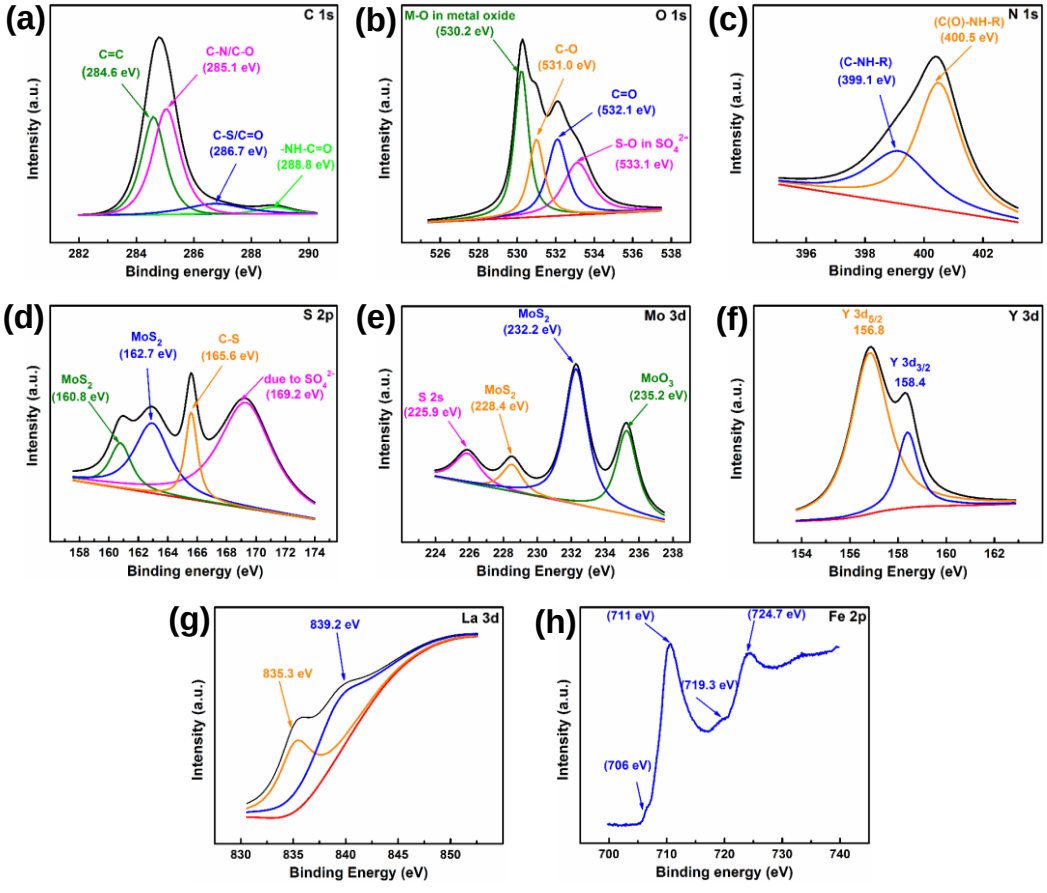

Figure 3.15. XPS spectra of the worn surface lubricated with (La-Y_2O_3)-MoS_2-(M-rGO) nanocomposite: (a) C 1s, (b) O 1s, (c) N 1s, (d) S 2p, (e) Mo 3d, (f) Y 3d, (g) La 3d spectra, and (h) Fe 2p spectra

The C 1s spectrum (Figure 3.15a) in the tribofilm revealing peaks at binding energy 284.6, 285.1, 286.7, 288.8 eV, appears to be approximately similar to that before the test.[19,22,61,62] Thus, the chemical state of carbon bonded to carbon, nitrogen, oxygen, and sulfur remains unaltered. The spectrum of O 1s displayed in Figure 3.15b shows four peaks. The peaks at 530.2, 531.0, 532.1, and 533.1 eV are indexed for M-O bonds of

metal oxides [Y(III)-O, La(III)-O and Fe(II/III)-O, Mo(VI)-O], C-O, C=O and –S(VI)-O bond of SO_4^{2-}, respectively.[7,43,57,70,71] The N 1s spectrum illustrated in Figure 3.15c exhibits the peaks for C-NH-R and C(O)NHR at 399.1 and 400.5 eV, respectively, as shown in the XPS spectrum before the antiwear test.[19]

In the S 2p spectrum (Figure 3.15d), besides three peaks at 160.8, 162.7, and 165.6 eV, an additional peak at 169.2 eV is also observed for sulfate as the oxidized sulfur under tribo conditions.[8,29,62,71] The interesting feature divulged in the molybdenum 3d spectrum (Figure 3.15e) is the presence of a new peak at 235.2 eV due to oxidation of Mo(IV) to MoO_3.[29,72] Substitution of oxygen at defects in MoS_2 nanosheets has produced MoO_3.[56] The other almost unchanged peaks for $Mo^{(IV)}$ and 3d ($3d_{5/2}$ and $3d_{3/2}$) are identified at 228.4 and 232.2 eV. Besides this, an additional peak appearing at 225.9 eV has been indexed for S 2s.[8] The yttrium 3d spectrum (Figure 3.15f) shows two peaks at a similar position (156.8, 158.4 eV) indicating the same chemical state after tribochemical interaction.[37,57] The peaks at 835.3, and 839.2 eV are apparent in the La 3d spectrum, Figure 3.15g. However, the peak at 835.3 eV is considered as characteristic of lanthanum again in +3 oxidation state as La_2O_3.[21,43,64] The appearance of distinct peaks for Fe $2p_{3/2}$ and Fe $2p_{1/2}$ in the Fe 2p spectrum at 711 and 724.7 eV respectively manifests formation of Fe_2O_3. The last peak has also been considered for iron sulfate.[71] Besides, extremely weak peaks at 706, 719.3 eV denote that Fe is almost absent in the native state.[71] Based on XPS studies, it may be stated that tribofilm is composed of adsorbed organic contents of M-rGO, Y_2O_3, La_2O_3, MoS_2, and tribochemically produced Fe_2O_3, iron sulfate, and MoO_3. The MoO_3 is itself triboactive, adds feasibility to sliding motion. Both MoO_3 and

iron sulfate help in adhering nanosheets on the tribosurface. Thus, the contents of tribofilm have interacted positively to yield spectacular triboactivity.[72]

3.3.2.7. Tribo-chemistry and mechanism of lubrication

For the tribological activity, the first and foremost, the additive has to adhere to the tribo surfaces facilitating tribofilm formation under the prevailing environment. The uniformity and strength of the *in situ* evolved tribochemical film are instrumental in interpreting the efficiency of the additive. The credit for the excellent performance of ternary additive is conferred to mutualistic interactions among the La-doped yttria nanoparticles, nanosheets of MoS_2, and methionine functionalized rGO. The M-rGO and MoS_2 carried over the layered structure throughout the lubrication process resulting in enhanced feasibility of sliding motion.[9,29] The NPs decorating the nanosheets helped in keeping the surfaces far apart[5,25,58] and preventing their reassembling and agglomeration.[8,25,58] In addition to this, NPs embellishing nanosheets have provided reinforcement and upgraded the dispersibility.[6,9,21,58] Functionalization of rGO by methionine has strengthened it and increased load-carrying capacity. They have also contributed towards improving poor adherence of rGO.[23] Concurrently, the agglomeration of nanoparticles is averted in the presence of nanosheets. The nanoparticles themselves have promoted lubrication by their nano-bearing behavior between the nanosheets or the moving surfaces.[5,21,58,73,74] The proximal surfaces have been rejuvenated by the tribo-sinterization of the NPs in the small cavities.[58,73,74] The rubbing action of NPs on the cuffed surface improves lubrication by providing finishing to the surface.[5,73,74] Besides this, the size of the NPs gets considerably contracted after

doping. The reduced size furnishes improved lubrication.[22] EDX analysis of the worn surface confirmed the existence of the constituent elements, C, N, O, S, Y, La, and Mo in the tribofillm. The XPS studies could enlighten on the additional chemical species formed after tribochemical oxidation, Fe_2O_3, MoO_3, and iron sulfate besides oxides of yttrium, lanthanum, and MoS_2.[29,71,72] The molybdenum trioxide assists in affixing the MoS_2 nanosheets while iron sulfate escalates the adsorption of nanosheets on the mating surfaces.[29,72] Thus, the cumulative effect of doped NPs, methionine functionalized rGO, and MoS_2 nanosheets have synergized the antiwear and antifriction efficiency of the nanocomposite through tribochemical products.

3.4. Conclusions

The auto-combustion method was followed to prepare the nanoparticles of yttria (Y_2O_3), and 7% lanthanum-doped yttria (La-Y_2O_3). A hydrothermal method was adopted to prepare MoS_2 nanosheets using ammonium heptamolybdate. The graphene oxide was prepared by modified Hummer's method and further functionalized by methionine to form M-rGO. The addition of M-rGO to the binary composite (La-Y_2O_3)-MoS_2 resulted in the formation of ternary nanocomposite (La-Y_2O_3)-MoS_2-(M-rGO). The structure and morphology of all of the synthesized additives, nanosheets, nanoparticles/doped nanoparticles, and binary/ternary nanocomposites were investigated by the techniques Raman, powder XRD, HR-SEM with EDX, and TEM/HR-TEM. The chemical states of different elements in the ternary nanocomposite were studied by XPS. The dispersions of nanohybrids in the base oil were found to be stable even after 48 h as studied by UV/vis spectroscopy. The antiwear and antifriction efficiencies of the individual additives in base

lube investigated on a four-ball tribo-tester according to ASTM D4172 and ASTM D5183 standards appear in ascending order Y_2O_3, MoS_2, M-rGO, and La-Y_2O_3. The La-Y_2O_3 nanoparticles and MoS_2 nanosheets exhibit enough tribological activity, but aggrandized activity is noted in the composite (La-Y_2O_3)-MoS_2. The lubricity of methionine functionalized rGO is well enhanced from the otherwise tribologically active GO nanosheets. Upon the addition of M-rGO to (La-Y_2O_3)-MoS_2, the activity is much improved. Thus, the robust synergy between nanoparticles and nanosheets has assured paramount activity. The wear track studies based on SEM and AFM authenticate the gradation discussed above. The Y_2O_3 nanoparticles participated in improving lubrication via rolling, polishing, and mending mechanisms. Nanoparticles/doped nanoparticles have reinforced the nanosheets of MoS_2/M-rGO, successfully aided in segregating them from one another, and hindered them from getting re-piled. The nanosheets have successively countered the agglomeration of nanoparticles. The incredible tribo-activity of the ternary composite (La-Y_2O_3)-MoS_2-(M-rGO) is accredited to intense interaction among the constituents as supported by XPS of the tribofilm.

3.5. References

(1) Gulzar, M.; Masjuki, H.H.; Kalam, M.A.; Varman, M.; Zulkifli, N.W.; Mufti, R.A.; Zahid, R. Tribological performance of nanoparticles as lubricating oil additives. *J. Nanoparticle Res.* **2016**, *18*(8), 1-25.

(2) Xiao, H.; Liu, S. 2D nanomaterials as lubricant additive: a review. *Mater. Des.* **2017**, *135*, 319-332.

(3) Zhai, W.; Zhou, K. Nanomaterials in Superlubricity. *Adv. Funct. Mater*. **2019**, *29*(28), 1-19.

(4) Kumar, B.; Verma, D.K.; Kavita; Rastogi, R.B. Tribological activity of ionic liquid stabilized calcium-doped ceria nanoparticles. *P. I. Mech. Eng. J-J Eng.* **2020**, 1350650120935005.

(5) Singh, A.; Chauhan, P.; Mamatha, T.G. A review on tribological performance of lubricants with nanoparticles additives. *Mater. Today Proc*. **2019**.

(6) Jia, X.; Huang, J.; Li, Y.; Yang, J.; Song, H. Monodisperse Cu nanoparticles@MoS_2 nanosheets as a lubricant additive for improved tribological properties. *Appl. Surf. Sci*. **2019**, *494*, 430-439.

(7) Song, H.; Wang, B.; Zhou, Q.; Xiao, J.; Jia, X. Preparation and tribological properties of MoS_2/graphene oxide composites. *Appl. Surf. Sci*. **2017**, *419*, 24-34.

(8) Yi, M.; Zhang, C. The synthesis of two-dimensional MoS_2 nanosheets with enhanced tribological properties as oil additives. *RSC Adv.* **2018**, *8*(17), 9564-9573.

(9) Nautiyal, H.; Kumari, S.; Khatri, O.P.; Tyagi, R. Copper matrix composites reinforced by rGO-MoS_2 hybrid: strengthening effect to enhancement of tribological

properties. *Compos. Part B Eng*. **2019**, *173*, 106931.

(10) Liu, Y.; Ge, X.; Li, J. Graphene lubrication. *Appl. Mater. Today* **2020**, *20*, 100662.

(11) Ge, X.; Li, J.; Luo, R.; Zhang, C.; Luo, J. Macroscale superlubricity enabled by the synergy effect of graphene-oxide nanoflakes and ethanediol. *ACS Appl. Mater. Interfaces* **2018**, *10*(47), 40863-40870.

(12) Ge, X.; Li, J.; Wang, H.; Zhang, C.; Liu, Y.; Luo, J. Macroscale superlubricity under extreme pressure enabled by the combination of graphene-oxide nanosheets with ionic liquid. *Carbon* **2019**, *151*, 76-83.

(13) Ma, Z.S.; Ding, H.L.; Liu, Z.; Cheng, Z.L. Preparation and tribological properties of hydrothermally exfoliated ultrathin hexagonal boron nitride nanosheets (BNNSs) in mixed NaOH/KOH solution. *J. Alloys Compd.* **2019**, *784*, 807-815.

(14) Rajendhran, N.; Palanisamy, S.; Periyasamy, P.; Venkatachalam, R. Enhancing of the tribological characteristics of the lubricant oils using Ni-promoted MoS_2 nanosheets as nano-additives. *Tribol. Int*. **2018**, *118*, 314-328.

(15) Chen, B.; Li, X.; Jia, Y.; Xu, L.; Liang, H.; Li, X.; Yang, J.; Li, C.; Yan, F. Fabrication of ternary hybrid of carbon nanotubes/graphene oxide/MoS_2 and its enhancement on the tribological properties of epoxy composite coatings. *Compos. Part A Appl. Sci. Manuf*. **2018**, *115*, 157-165.

(16) Qiao, W.; Wang, L.; Ye, B.; Li, G.; Li, J. Electrochemical behavior of palmatine and its sensitive determination based on an electrochemically reduced L-methionine functionalized graphene oxide modified electrode. *Analyst* **2015**, *140*(23), 7974-

7983.

(17) Kuila, T.; Bose, S.; Mishra, A. K.; Khanra, P.; Kim, N. H.; Lee, J. H. Chemical functionalization of graphene and its applications. Prog. Mater. Sci. **2012**, *57*(7), 1061−1105.

(18) Georgakilas, V.; Otyepka, M.; Bourlinos, A.B.; Chandra, V.; Kim, N.; Kemp, K.C.; Hobza, P.; Zboril, R.; Kim, K.S. Functionalization of graphene: covalent and non-covalent approaches, derivatives and applications. *Chem. Rev.* **2012**, *112*(11), 6156-6214.

(19) Gan, C.; Liang, T.; Li, W.; Fan, X.; Zhu, M. Amine-terminated ionic liquid modified graphene oxide/copper nanocomposite toward efficient lubrication. *Appl. Surf. Sci*. **2019**, *491*, 105-115.

(20) Meng, Y.; Su, F.; Chen, Y. Au/graphene oxide nanocomposite synthesized in supercritical CO_2 fluid as energy efficient lubricant additive. *ACS Appl. Mater. Interfaces*. **2017**, *9*(45), 39549-39559.

(21) Hou, X.; Yang, C.; He, J.; Li, Z.; Zhang, Z. Preparation and tribological properties of lanthanum trifluoride nanoparticles-decorated graphene oxide nanosheets. *Ind. Eng. Chem. Res*. **2015**, *54*(17), 4773-4780.

(22) Verma, D.K.; Kumar, B.; Kavita; Rastogi, R.B. Zinc oxide and magnesium-doped zinc oxide-decorated nanocomposites of reduced graphene oxide as friction and wear modifiers. *ACS Appl. Mater. Interfaces* **2018**, *11*(2), 2418-2430.

(23) Jaiswal, V.; Umrao, S.; Rastogi, R.B.; Kumar, R.; Srivastava, A. Synthesis, characterization, and tribological evaluation of TiO_2-reinforced boron and nitrogen

co-doped reduced graphene oxide based hybrid nanomaterials as efficient antiwear lubricant additives. *ACS Appl. Mater. Interfaces*. **2016**, *8*(18), 11698-11710.

(24) Verma, D.K.; Kuntail, J.; Kumar, B.; Singh, A.K.; Shukla, N.; Kavita; Sinha, I.; Rastogi, R.B. Amino Borate-Functionalized Reduced Graphene Oxide Further Functionalized with Copper Phthalocyanine Nanotubes for Reducing Friction and Wear. *ACS Appl. Nano Mater.* **2020**, 3(6), 5530-5541.

(25) Verma, D.K.; Shukla, N.; Kumar, B.; Singh, A.K.; Shahu, K.; Yadav, M.; Rhee, K.Y.; Rastogi, R.B. Synergistic tribo-activity of nanohybrids of zirconia/cerium-doped zirconia nanoparticles with nano lamellar reduced graphene oxide and molybdenum disulfide. *Nanomaterials* **2020**, *10*(4), 707.

(26) Mallakpour, S.; Abdolmaleki, A.; Borandeh, S. Covalently functionalized graphene sheets with biocompatible natural amino acids. *Appl. Surf. Sci*. **2014**, *307*, 533-542.

(27) Rambabu, G.; Bhat, S.D. Amino acid functionalized graphene oxide based nanocomposite membrane electrolytes for direct methanol fuel cells. *J. Memb. Sci*. **2018**, *551*, 1-11.

(28) Song, W.; Yan, J.; Ji, H. Tribological study of SOCNTs@MoS_2 composite as a lubricant additive: synergistic effect. *Ind. Eng. Chem. Res*. **2018**, *57*(20), 6878-6887.

(29) Xu, Y.; Peng, Y.; Dearn, K.D.; Zheng, X.; Yao, L.; Hu, X. Synergistic lubricating behaviors of graphene and MoS_2 dispersed in esterified bio-oil for steel/steel contact. *Wear* **2015**, *342*, 297-309.

(30) Wu, P.R.; Feng, Y.M.; Ge, T.; Kong, Y.C.; Ma, Z.S.; Liu, Z.; Cheng, Z.L. An

investigation on tribological properties of the chemically capped zinc borate (ZB)/MoS_2 nanocomposites in oil. *J. Ind. Eng. Chem*. **2018**, *63*, 157-167.

(31) Zheng, X.; Xu, Y.; Geng, J.; Peng, Y.; Olson, D.; Hu, X. Tribological behavior of Fe_3O_4/MoS_2 nanocomposites additives in aqueous and oil phase media. *Tribol. Int*. **2016**, *102*, 79-87.

(32) Yu, L.; Zhang, L.; Ye, F.; Sun, M.; Cheng, X.; Diao, G. Preparation and tribological properties of surface-modified nano-Y_2O_3 as additive in liquid paraffin. *Appl. Surf. Sci*. **2012**, *263*, 655-659.

(33) Rong, J.; Yang, K.; Zhao, H.; Liu, C.; Zhuang, Y.; Tao, S. Tribological performance of plasma sprayed Al_2O_3-Y_2O_3 composite coatings. *Surf. Coat. Technol*. **2016**, *302*, 487-494.

(34) Li, J.F.; Liao, H.; Wang, X.Y.; Normand, B.; Ji, V.; Ding, C.X.; Coddet, C. Improvement in wear resistance of plasma sprayed yttria stabilized zirconia coating using nanostructured powder. *Tribol. Int*. **2004**, *37*(1), 77-84.

(35) Gan, L.; Park, Y.J.; Kim, H.; Kim, J.M.; Ko, J.W.; Lee, J.W. Effects of pre-sintering and annealing on the optical transmittance of Zr-doped Y_2O_3 transparent ceramics fabricated by vacuum sintering conjugated with post-hot-isostatic pressing. *Ceram. Int*. **2015**, *41*(8), 9622-9627.

(36) Huang, Y.; Jiang, D.; Zhang, J.; Lin, Q. Precipitation synthesis and sintering of lanthanum doped yttria transparent ceramics. *Opt. Mater*. **2009**, *31*(10), 1448-1453.

(37) Mariscal-Becerra, L.; Vázquez-Arreguín, R.; Balderas, U.; Carmona-Téllez, S.; Murrieta Sánchez, H.; Falcony, C. Luminescent characteristics of layered yttrium

oxide nano-phosphors doped with europium. *J. Appl. Phys*. **2017**, *121*(12), 125111.

(38) Shirinparvar, S.; Razavi, R.S.; Davar, F.; Loghman-Estarki, M.R.; Hajizadeh-Oghaz, M.; Ghorbani, S. Synthesis, characterization, and optical properties of $Zr^{+4}/La^{+3}/Nd^{+3}$ tri-doped yttria nanopowder by sol-gel combustion method. *Ceram. Int*. **2016**, *42*(9), 10551-10558.

(39) Nath, S.; Sinha, N.; Basu, B. Microstructure, mechanical, and tribological properties of microwave sintered calcia-doped zirconia for biomedical applications. *Ceram. Int*. **2008**, *34*(6), 1509-1520.

(40) Ghaemi, M.H.; Reichert, S.; Krupa, A.; Sawczak, M.; Zykova, A.; Lobach, K.; Sayenko, S.; Svitlychnyi, Y. Zirconia ceramics with additions of alumina for advanced tribological and biomedical applications. *Ceram. Int*. **2017**, *43*(13), 9746-9752.

(41) Kalyani; Rastogi, R.B.; Kumar, D. Synthesis, characterization, and tribological evaluation of SDS-stabilized magnesium-doped zinc oxide ($Zn_{0.88}Mg_{0.12}O$) nanoparticles as efficient antiwear lubricant additives. *ACS Sustain. Chem. Eng*. **2016**, *4*(6), 3420-3428.

(42) Charde, S.J.; Sonawane, S.S.; Rathod, A.P.; Sonawane, S.H.; Shimpi, N.G.; Parate, V.R. Copper-doped zinc oxide nanoparticles: influence on thermal, thermo mechanical, and tribological properties of polycarbonate. *Polym. Compos*. **2018**, *39*(S3), 1398-1406.

(43) Kecheng, G.U.; Boshui, C.H.; Yong, C.H. Preparation and tribological properties of lanthanum-doped TiO_2 nanoparticles in rapeseed oil. *J. Rare Earths* **2013**, *31*(6),

589-594.

(44) Yadgarov, L.; Petrone, V.; Rosentsveig, R.; Feldman, Y.; Tenne, R.; Senatore, A. Tribological studies of rhenium doped fullerene-like MoS_2 nanoparticles in boundary, mixed, and elasto-hydrodynamic lubrication conditions. *Wear* **2013**, *297*(1-2), 1103-1110.

(45) Shi, Q.; Tang, H.; Zhu, H.; Tang, G.; Zhang, K.; Zhang, H.; Li, C. Synthesis and tribological properties of Ti-doped $NbSe_2$ nanoparticles. *Chalcogenide Lett*. **2014**, *11*(5), 199-207.

(46) Huang, Y.; Jiang, D.; Zhang, J.; Lin, Q. Fabrication of transparent lanthanum-doped yttria ceramics by combination of two-step sintering and vacuum sintering. *J. Am. Ceram. Soc.* **2009**, *92*(12), 2883-2887.

(47) Huang, Y.; Jiang, D.; Zhang, J.; Lin, Q. Fabrication of lanthanum doped yttria transparent ceramics. *Chinese Sci. Bull*, **2009**, *54*(12), 2143-2146.

(48) Hajizadeh-Oghaz, M.; Razavi, R.S.; Barekat, M.; Naderi, M.; Malekzadeh, S.; Rezazadeh, M. Synthesis and characterization of Y_2O_3 nanoparticles by sol-gel process for transparent ceramics applications. *J. Sol-Gel Sci. Technol*. **2016**, *78*(3), 682-691.

(49) Huang, Y.; Jiang, D.; Zhang, J.; Lin, Q. Precipitation synthesis and sintering of lanthanum doped yttria transparent ceramics. *Opt. Mater*. **2009**, *31*(10), 1448-1453.

(50) Liu, L.; Jiao, S.; Peng, Y.; Zhou, W. A green design for lubrication: multifunctional system containing Fe_3O_4@MoS_2 nanohybrid. *ACS Sustain. Chem. Eng*. **2018**, *6*(6), 7372-7379.

(51) Hu, Z.; Li, C.; Nie, R.; Li, Y.Q.; Tang, J.X.; Deng, X. Biomaterial functionalized graphene oxides with tunable work function for high sensitive organic photodetectors. *RSC Adv*. **2015**, *5*(120), 99431-99438.

(52) Song, Y.; Cao, L.; Yu, J.; Zhang, S.; Chen, S.; Jiang, Y. Amino-functionalized graphene oxide blend with monoethanolamine for efficient carbon dioxide capture. *J. Alloys Compd*. **2017**, *704*, 245-253.

(53) Zhu, H.; Zhang, Y.; Zhang, L.; Yu, T.; Zhang, K.; Jiang, H.; Wu, L.; Wang, S. Highly photostable and biocompatible graphene oxides with amino acid functionalities. *J. Mater. Chem. C* **2014**, *2*(34), 7126-7132.

(54) Rao, C.N.; Venkataraghavan, R.; Kasturi, T.R. Contribution to the infrared spectra of organosulphur compounds. *Can. J. Chem*. **1964**, *42*(1), 36-42.

(55) Meng, N.; Zhou, Y.; Nie, W.; Chen, P. Synthesis of CdS-decorated rGO nanocomposites by reflux condensation method and its improved photocatalytic activity. *J. Nanoparticle Res*. **2016**, *18*(8), 241.

(56) Rawat, S.S.; Harsha, A.P.; Agarwal, D.P.; Kumari, S.; Khatri, O.P. Pristine and alkylated MoS_2 nanosheets for enhancement of tribological performance of paraffin grease under boundary lubrication regime. *J. Tribol*. **2019**, *141*(7).

(57) Lin, L.; Starostin, S.A.; Li, S.; Khan, S.A.; Hessel, V. Synthesis of yttrium oxide nanoparticles via a facile microplasma-assisted process. *Chem. Eng. Sci*. **2018**, *178*, 157-166.

(58) Paul, G.; Hirani, H.; Kuila, T.; Murmu, N.C. Nanolubricants dispersed with graphene and its derivatives: an assessment and review of the tribological

performance. *Nanoscale* **2019**, *11*(8), 3458-3483.

(59) Belachew, N.; Meshesha, D.S.; Basavaiah, K. Green syntheses of silver nanoparticle decorated reduced graphene oxide using L-methionine as a reducing and stabilizing agent for enhanced catalytic hydrogenation of 4-nitrophenol and antibacterial activity. *RSC Adv*. **2019**, *9*(67), 39264-39271.

(60) Kruk, A. Optical and structural properties of arc melted Ce or Pr-doped Y_2O_3 transparent ceramics. *Ceram. Int*. **2017**, *43*(18), 16909-16914.

(61) Kumar, B.; Verma, D.K.; Singh, A.K.; Kavita; Shukla, N.; Rastogi, R.B.. Nanohybrid Cu@ C: synthesis, characterization and application in enhancement of lubricity. *Compos. Interfaces* **2019**, 1-18.

(62) Yang, Z.; Dai, Y.; Wang, S.; Cheng, H.; Yu, J. In situ incorporation of a S, N doped carbon/sulfur composite for lithium sulfur batteries. *RSC Adv*. **2015**, *5*(95), 78017-78025.

(63) Jin, F.; Yang, G.; Song, S.; Zhang, S.; Yu, L.; Zhang, P. Synthesis of nanostructured lanthanum fluoborate modified by oleylamine and evaluation of its tribological properties as a lubricating additive in synthetic ester. *Surf. Interface Anal*. **2016**, *48*(10), 1033-1039.

(64) Jia, Z.; Xia, Y. Hydrothermal synthesis, characterization, and tribological behavior of oleic acid-capped lanthanum borate with different morphologies. *Tribol. Lett*. **2011**, *41*(2), 425-434.

(65) Liu, Z.; Shu, D.; Li, P.; Cheng, X. Tribology study of lanthanum-treated graphene oxide thin film on silicon substrate. *RSC Adv*. **2014**, *4*(31), 15937-15944.

(66) Zhou, Q.; Huang, J.; Wang, J.; Yang, Z.; Liu, S.; Wang, Z.; Yang, S. Preparation of a reduced graphene oxide/zirconia nanocomposite and its application as a novel lubricant oil additive. *RSC Adv.* **2015**, *5*(111), 91802-91812.

(67) Bai, G.; Wang, J.; Yang, Z.; Wang, H.; Wang, Z.; Yang, S. Preparation of a highly effective lubricating oil additive–ceria/graphene composite. *RSC Adv.* **2014**, *4*(87), 47096-47105.

(68) Yu, W.; Xie, H. A review on nanofluids: preparation, stability mechanisms, and applications. *J. Nanomater.* **2012**.

(69) Kumar, R.; Prakash, B.; Sethuramiah, A. A systematic methodology to characterise the running-in and steady-state wear processes. *Wear* **2002**, *252*(5−6), 445−453.

(70) Hou, X.; He, J.; Yu, L.; Li, Z.; Zhang, Z.; Zhang, P. Preparation and tribological properties of fluorosilane surface-modified lanthanum trifluoride nanoparticles as additive of fluoro silicone oil. *Appl. Surf. Sci*. **2014**, *316*, 515-523.

(71) Xu, Y.; Hu, E.; Hu, K.; Xu, Y.; Hu, X. Formation of an adsorption film of MoS_2 nanoparticles and dioctyl sebacate on a steel surface for alleviating friction and wear. *Tribol. Int.* **2015**, *92*, 172-183.

(72) Zhao, J.; He, Y.; Wang, Y.; Wang, W.; Yan, L.; Luo, J. An investigation on the tribological properties of multilayer graphene and MoS_2 nanosheets as additives used in hydraulic applications. *Tribol. Int*. **2016**, *97*, 14-20.

(73) Kumar, B.; Verma, D.K.; Shukla, N.; Singh, A.K.; Rastogi, R.B. Ionic liquid stabilized Ag@C composite for improvement of triboactivity. *J. Mol. Liq.* **2020**,

113012.

(74) Tang, Z.; Li, S. A review of recent developments of friction modifiers for liquid lubricants (2007–present). *Curr. Opin. Solid State Mater. Sci*. **2014**, *18*(3), 119-139.